Influence of Enhanced Abyssal Diapycnal Mixing on Stratification and the Ocean Overturning Circulation

A. MASHAYEK AND R. FERRARI

Massachusetts Institute of Technology, Cambridge, Massachusetts

M. NIKURASHIN

Institute for Marine and Antarctic Studies, University of Tasmania, Hobart, Tasmania, and ARC Centre of Excellence for Climate System Science, Sydney, New South Wales, Australia

W. R. PELTIER

University of Toronto, Toronto, Ontario, Canada

(Manuscript received 24 February 2015, in final form 28 May 2015)

ABSTRACT

The meridional overturning circulation (MOC) is composed of interconnected overturning cells that transport cold dense abyssal waters formed at high latitudes back to the surface. Turbulent diapycnal mixing plays a primary role in setting the rate and patterns of the various overturning cells that constitute the MOC. The focus of the analyses in this paper will be on the influence of sharp vertical variations in mixing on the MOC and ocean stratification. Mixing is enhanced close to the ocean bottom topography where internal waves generated by the interaction of tides and geostrophic motions with topography break. It is shown that the sharp vertical variations in mixing lead to the formation of three layers with different dynamical balances governing meridional flow. Specifically, an abyssal bottom boundary layer forms above the ocean floor where mixing is largest and hosts the northward transport of the heaviest waters from the southern channel to the closed basins. A deep layer forms above the bottom layer in which the upwelled waters return south. A third adiabatic layer lies above the other two. While the adiabatic layer has been studied in detail in recent years, the deep and bottom layers are less appreciated. It is shown that the bottom layer, which is not resolved or allowed for in most idealized models, must be present to satisfy the no flux boundary condition at the ocean floor and that its thickness is set by the vertical profile of mixing. The deep layer spans a considerable depth range of the ocean within which the stratification scale is set by mixing, in line with the classic view of Munk in 1966.

1. Introduction

On a global scale, the ocean deep circulation can be described in terms of a number of interconnected meridional overturning circulations (MOCs). Talley (2013) summarizes the overall MOC as a flow of North Atlantic Deep Water (NADW) sinking in the Northern Hemisphere and flowing along isopycnals all the way to the Southern Ocean, where it comes to the surface to be converted into Antarctic Bottom Water (AABW), primarily along the coast of Antarctica. The AABW then sinks into the abyss and fills the bottom of all the oceans basins. In the basins, AABW is mixed by turbulent processes with the overlying deep waters in the Atlantic, Pacific, and Indian Oceans and returns back to the Southern Ocean as a lighter water mass. Once at the surface these deep waters are converted into intermediate waters that flow to the North Atlantic, thereby closing the MOC. The role of turbulent mixing in setting the rate and patterns of the MOC is a current topic of intense debate and is the focus of the present study.

Talley's (2013) heuristic description of the MOC, while highly simplified, is still too complex to be captured by analytical models that lend themselves to straightforward analysis. Therefore, over the past few decades, many studies have attempted to gain basic understanding of the physical processes that set the deep stratification and rate of the MOC by considering highly

Corresponding author address: Ali Mashayek, Massachusetts Institute of Technology, 77 Massachusetts Ave., Cambridge, MA 02139. E-mail: ali_mash@mit.edu

DOI: 10.1175/JPO-D-15-0039.1

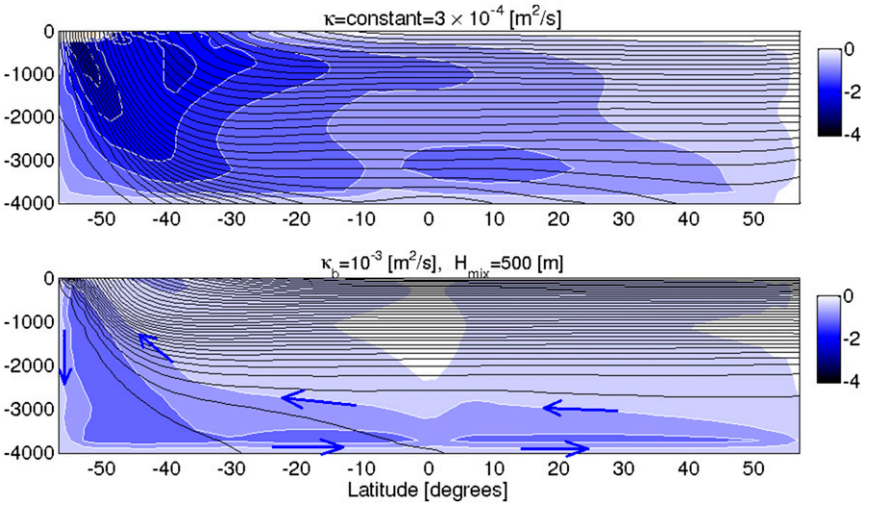

FIG. 1. Zonally averaged meridional overturning streamfunction [Sverdrups (Sv; 1 Sv = $10^6\,m^3\,s^{-1}$)] overlaid by isopycnals in the deep ocean. (top) A case with a constant diapycnal diffusivity of $\kappa = 3 \times 10^{-4}\,m^2\,s^{-1}$; (bottom) a case with κ decaying from $10^{-3}\,m^2\,s^{-1}$ at the bottom to $10^{-5}\,m^2\,s^{-1}$ at the top with a decay scale of 500 m. The arrows represent the sense of the circulation. The model is discussed in detail in section 3.

idealized geometries. A standard choice has been to consider a flat-bottom ocean basin connected to a reentrant zonally periodic channel in the south, representing the Southern Ocean latitudes where there is no zonal blocking by continents. A number of studies in this geometrical configuration have found that the lower branch of the MOC, corresponding loosely to the flow of AABW, is strongly influenced by the rate of abyssal mixing (Ito and Marshall 2008, hereinafter IM08; Nikurashin and Vallis 2011, hereinafter NV11).

Turbulent mixing in the idealized studies is typically represented as a constant diapycnal diffusivity κ. However, there is extensive observational evidence that the diapycnal diffusivity is enhanced at the bottom of the ocean and that it also varies in the horizontal (e.g., Waterhouse et al. 2014). The bottom enhancement reflects the generation of energetic turbulence by tides and geostrophic flows impinging over topography (e.g., Wunsch and Ferrari 2004; Nikurashin and Ferrari 2010b,a). The vertical decay scale of κ is estimated to be of order of a few hundred meters (Lumpkin and Speer 2007; Ganachaud 2003; Melet et al. 2013; Waterhouse et al. 2014). In this work, we explore the implications of the downward increase of κ on the abyssal ocean stratification and MOC, leaving the implications of horizontal variations for future work.

To illustrate the importance of the vertical structure in κ on the MOC, in Fig. 1 we compare two numerical solutions of the ocean circulation in an idealized geometry with a basin and a circumpolar channel, one using a constant κ profile and the other using a κ profile increasing toward the ocean bottom. The model used to obtain the solutions will be discussed in detail later and at this point it suffices to state that the MOC plots in the figure are zonal integrals of three-dimensional solutions obtained in a rectangular geometry representing an ocean basin connected to a reentrant channel at the south over which westerly winds blow (seen later in Fig. 6). The buoyancy forcing at the surface is such that deep waters form only at the southern end of the channel, mimicking an Indo-Pacific-like MOC. The top panel in the figure corresponds to a simulation that uses a constant diffusivity $\kappa = 3 \times 10^{-4}\,m^2\,s^{-1}$, while the bottom panel is from a simulation with a profile of κ that decays exponentially from a bottom value of 1×10^{-3} to $1 \times 10^{-5}\,m^2\,s^{-1}$ at the surface over an e-folding scale of $H_{\rm mix} = 500$ m. The two profiles are chosen so that their vertical integrals are similar. In the simulation with a decaying profile of κ, the MOC is weaker and its maximum closer to the ocean bottom. The bottom stratification is also weaker. These are substantial changes and suggest that a theory of abyssal ocean stratification and circulation must account for vertical variations in κ.

In this paper our focus will be upon three main points. We show that the sharp upward decay of mixing away from the ocean bottom leads to the formation of three distinct layers below the depth of the surface wind-driven gyres. The three layers are identified by different dynamical balances: an abyssal bottom boundary layer (ABL), a deep layer (DL), and an upper adiabatic layer (AL). The abyssal boundary layer forms above the ocean floor where mixing is largest. This layer will be

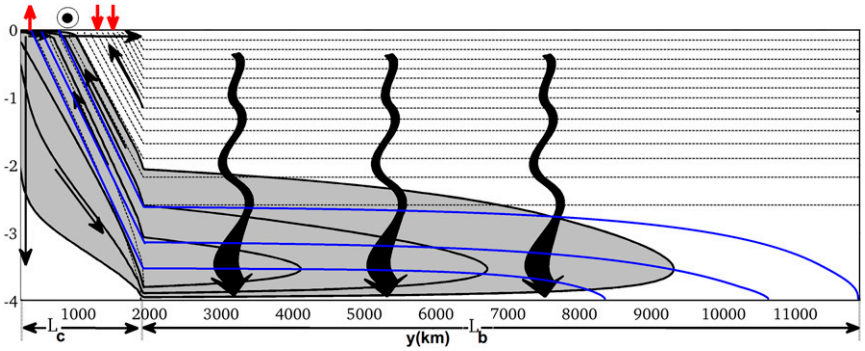

FIG. 2. Schematic of the zonally averaged circulation. At the surface of the reentrant channel ($0 < y < L_c$), red arrows represent heat flux to the atmosphere in such a form that leads to deep-water formation at the southern edge, while the arrowhead facing out of the page represents the wind direction. Thick curly arrows in the basin interior represent downward-enhancing diapycnal diffusion of buoyancy. Thin dashed lines represent flat isopycnals in the low mixing depth range and curved blue lines represent isopycnals influenced by enhanced mixing in the abyssal boundary layer.

shown to be host to strong basinwide gyres that transport the heaviest waters from the channel into the basin to the north, where they upwell through mixing. The upwelled waters return south in the DL through a combination of weaker ocean gyres in the basin and Ekman suction in the channel. Mixing is a key in the dynamics of both ABL and DL, in accord with the view of Munk and Wunsch (1998) in their abyssal recipes' analysis. The third layer lies on top of the DL, where mixing is weak and the meridional circulation is nearly adiabatic and maintained through a balance between the wind forcing and the slumping of density surfaces through baroclinic instability in the channel, as described in Wolfe and Cessi (2011).

This paper is organized as follows: In section 2, we describe the theoretical framework for our analysis and present scaling arguments to determine the specific processes that are responsible for controlling the abyssal circulation and stratification. The theoretical predictions are compared with idealized numerical experiments in section 3. Section 4 presents our conclusions.

2. Theoretical analysis

a. Problem formulation

We begin by considering the zonally averaged circulation in an idealized ocean schematically sketched in Fig. 2. The domain consists of two primary sections: (i) a circumpolar channel of meridional extent L_c, which is assumed to be zonally periodic and mimics the reentrant flow of the Southern Ocean at latitudes not blocked by lateral boundaries, and (ii) a closed basin to the north of the channel of meridional extent L_b, which represents the ocean basins bounded by continents. This idealized setup is forced at the surface by restoring to the surface temperature profile (shown below in Fig. 6) over a time scale of 1 month and a depth of 10 m, which leads to waters sinking only at the southern end of the channel. Thus, the model is best thought of as an idealization of the meridional circulation in the Indo-Pacific Ocean.

The circulation is characterized by dense water formation at the southern edge of the domain, resulting in an abyssal northward flow along the ocean floor from the southern channel to the ocean basin into the north. Once in the basin, diapycnal mixing resulting from wave breaking (illustrated by curly arrows) provides the energy for abyssal waters to upwell and then find their way back to the reentrant channel as deep waters. The thin dashed lines in the figure represent nearly horizontal isopycnals that lie above the enhanced mixing region in the abyss. In the enhanced mixing region, isopycnals, shown by blue lines, bend down. Our schematic distinction between two regions of flat and curved isopycnals is supported by hydrographic maps of isopycnals in the real ocean, illustrated in Fig. 3, and by the theoretical requirement that isopycnals intersect the bottom boundary at right angles in order to satisfy the no flux boundary condition. The latter point will be discussed in detail in section 2c.

The zonally averaged circulation in a 3D ocean is best described through the transformed Eulerian-mean (TEM) framework (Andrews and McIntyre 1976; Marshall and Radko 2003; Plumb and Ferrari 2005). In this framework, the residual streamfunction ψ is related to the meridional and vertical residual velocities through $(v^*, w^*) = (-\psi_z, \psi_y)$, where v^* and w^* represent the residual velocities given by the sum of the Eulerian

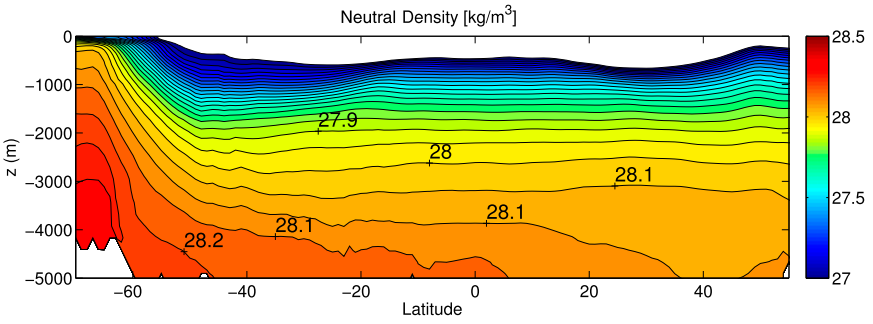

FIG. 3. Neutral density isosurfaces zonally averaged over the Pacific basin, calculated from the WOCE dataset (Gouretski and Koltermann 2004), illustrating the abyssal bottom layer in which isopycnals are curved down due to enhanced abyssal mixing.

mean and eddy-induced velocities.[1] The zonally averaged equations governing the zonal momentum and buoyancy budgets in the limit of small Rossby number and in steady-state form are (Marshall and Radko 2003)

$$\psi = \overline{\psi} + \psi_{\text{eddy}} = -\frac{\overline{\tau}}{f\rho_0} + \frac{1}{f\rho_0}\overline{p}_x + K_e s_b, \quad \text{and} \tag{1}$$

$$(\psi\overline{b}_z)_y - (\psi\overline{b}_y)_z = \partial_z(\kappa\overline{b}_z), \tag{2}$$

where f is the latitude-dependent Coriolis parameter, $\overline{p}$ is the zonally averaged pressure, $\overline{\tau}$ is the zonally averaged surface wind stress, K_e is the isopycnal eddy diffusivity, and $s_b = -\overline{b}_y/\overline{b}_z$ is the slope of the zonally averaged isopycnals. Following Gent and McWilliams (1990), the eddy circulation is assumed to be proportional to the isopycnal slope times K_e. Equations (1) and (2) are subject to boundary conditions of no normal flow through boundaries, no buoyancy flux through side and bottom boundaries, and the prescription of the surface buoyancy (representing the fast restoring to atmospheric temperatures) at the surface.

b. The southern channel

In the reentrant channel the MOC is the residual of an Eulerian-mean clockwise overturning circulation driven by surface westerly winds and an eddy-induced counterclockwise overturning circulation, which represents the slumping of isopycnals through baroclinic instability (Marshall and Radko 2003). Because of the zonal periodicity in the channel, the pressure gradient term on the right-hand side (RHS) of (1) drops out. Furthermore, NV11 showed that while the diffusive term in the buoyancy budget is of the same order as the advective terms in the ocean basin, in the channel it is smaller by a factor of L_c/L_b, the ratio of the channel meridional width to that of the basin. Since $L_c/L_b \sim O(0.1)$, the RHS of (2) may be ignored to the leading order in the channel. Thus, (1) and (2) reduce to

$$\psi = -\frac{\tau}{f\rho_0} + K_e s_b, \quad \text{and} \tag{3}$$

$$(\psi b_z)_y - (\psi b_y)_z \approx 0, \tag{4}$$

where here and in the following we drop the overbars. Equations (3) and (4) imply that, to leading order, the MOC in the channel is driven by the competing forces of winds and eddies, and the streamlines follow isopycnals (Marshall and Radko 2006; NV11).

While mixing plays a secondary role in the buoyancy budget in the channel, as discussed above, it will be shown that it plays a primary role in the basin where it acts to diffuse isopycnals downward. In order for channel isopycnals to match the basin solution at the interface, they thus have to steepen near the boundary, leading to enhanced eddy circulation. For large slopes, $\psi_{\text{eddy}} \gg \overline{\psi}$, a limit supported by the numerical simulations that we will discuss in the next section. In the real ocean abyss, this scaling is even more likely to hold because the Southern Ocean wind stress is partly balanced by a topographic form drag, so that the effective stress experienced by the water is substantially reduced below the depth of 2000 m (IM08). Therefore, the abyssal equations for the channel are to a good approximation

$$\psi \approx K_e s_b, \quad \text{and} \tag{5}$$

$$(\psi b_z)_y - (\psi b_y)_z \approx 0. \tag{6}$$

c. The ocean basin: Abyssal boundary layer

The ABL above the ocean floor where isopycnals intersect the ocean bottom is, perhaps, an unappreciated key element of the MOC. The zonally averaged models, reviewed above, which assume that density surfaces are

[1] The residual circulation is often written as $\psi^\dagger$ in the literature. Since we will be primarily concerned with the residual circulation herein, we omit the † and use ψ alone.

essentially flat in the ocean basins, inadvertently ignore the ABL. In such models, the abyssal ocean cannot maintain any stratification, as can be easily illustrated. If $b_y = 0$, the buoyancy budget in (2) reduces to $\psi_y b_z \approx (\kappa b_z)_z$, as assumed, for example, in NV11. Integrating this buoyancy budget from the ocean bottom at $z = -D$ to some arbitrary level z gives an expression for the stratification:

$$b_z = \frac{\mathcal{B}}{\kappa} \exp\left(\int_{-D}^{z} \frac{\psi_y}{\kappa} dz' \right), \tag{7}$$

where $\mathcal{B} = \kappa b_z|_{z=-D}$ is the buoyancy flux through the ocean floor. Thus, if one imposes a zero-flux boundary condition at the ocean floor, a common and reasonable assumption that ignores the weak geothermal flux, the stratification is predicted to vanish throughout the water column. One must relax the $b_y = 0$ assumption in the vicinity of the ocean floor and allow for the ABL in order to obtain solutions with nonzero abyssal stratification.

To obtain expressions for MOC and stratification in the ABL, we note that the ABL is defined as the abyssal layer where b_z remains small enough that $|\partial_z(\psi b_y)| \gg |\partial_y(\psi b_z)|$, and thus the buoyancy budget reduces to[2]

$$-\partial_z(\psi b_y) = \partial_z(\kappa b_z). \tag{8}$$

Integrating in z, we obtain a relationship between the MOC and the stratification as

$$\psi \approx -\kappa \frac{b_z}{b_y}, \tag{9}$$

where we have used the fact that $\psi = 0$ at $z = -D$. Furthermore, b_y in the basin may be substituted by $\Delta b/L$, where Δb represents the density difference across the vertical extent of ABL at the channel–basin interface and L is the horizontal distance between the intersect of that isopycnal with the ocean floor and the channel–basin interface (shown later in Fig. 5). Thus, (9) reduces to

$$\psi \Delta b \approx -\kappa_b b_z L, \tag{10}$$

which states that the downward diffusion of heat into the ABL is balanced by a horizontal flow that takes water into progressively lighter density classes (for a formal derivation see Lund et al. 2011, their appendix A). In the absence of a lateral density gradient b_y, such a balance cannot arise. IM08 obtained an equation similar to (9) but with L replaced by the width of the channel; their solution is only valid in the limit when κ is so large that the MOC closes before reaching the basin.

The expression for ψ in the basin given in (10) must match the solution in the channel at the channel–basin interface. According to (5), the channel momentum budget in the limit of steep isopycnal slopes, characteristic of the ABL, gives $\psi \sim -K_e b_y/b_z$. Substituting for b_y with $\Delta b/l$ (where here l represents the meridional stratification scale in the channel), we obtain

$$\psi \approx -K_e \frac{\Delta b}{l} \frac{1}{b_z}. \tag{11}$$

Matching this expression with the one in (10), we can solve for both stratification and MOC:

$$h_{\mathrm{ABL}} \approx \sqrt{\frac{\kappa_b}{K_e} L l}, \tag{12}$$

and

$$\psi_{\mathrm{ABL}} \approx -\sqrt{\frac{L}{l} K_e \kappa_b}. \tag{13}$$

The latter is similar to the expression discussed in NV11, with the important difference that in NV11, L was replaced by the basin meridional length L_b because of the flat isopycnal assumption. Hence, our analysis extends NV11 by taking into account the abyssal bending of isopycnals due to enhanced mixing (i.e., nonzero b_y), thereby allowing for a horizontal abyssal stratification to exist, implying $L < L_b$. But we do not have a closed theory because we do not have a scaling for L based on external parameters. According to (13), as one moves toward to ocean floor, $L \to 0$ and so does the circulation. Furthermore, (13) shows that the circulation in the bottom layer would not exist in the absence of turbulent mixing.

It is important to note that (12) and (13) are strictly valid at the channel–basin interface where, by definition, they are valid for both the channel and basin. The numerical simulations will show that b_y remains small (while not negligible) in the basin except close to the northern boundary. So, (12) applies also within the basin, north of the interface. Furthermore, within the idealized theoretical framework of the paper, $\partial_y \psi_{\mathrm{ABL}} = w_{\mathrm{ABL}}$ is small in the ABL because of the no normal flow boundary condition at the bottom boundary. Thus, ψ_{ABL} also varies weakly with y in the basin. It is unclear whether (13) holds in a more realistic flow configuration with uneven bottom topography. Nevertheless, (13) will

[2] The LHS of (8) may alternatively be written in form of $vb_y - \psi b_{yz}$. We verified that $vb_y \gg \psi b_{yz}$ and so (8) also implies that $vb_y \gg wb_z$.

prove useful for interpreting the results of the numerical experiments in the next section.

d. The ocean basin: Deep layer

The northward-flowing ABL waters return south in a layer sandwiched between the ABL and the upper ocean. This DL is characterized by enhanced mixing (smaller than in the ABL but larger than in the adiabatic layer above) and smaller isopycnal slopes such that at leading order

$$\psi_y b_z \approx (\kappa b_z)_z, \tag{14}$$

that is, b_y is sufficiently small that b can be assumed to be only a function of z. Notice that in the absence of y dependence in b (14) implies

$$w = \psi_y \approx \frac{\psi}{L_b} \approx \frac{(\kappa b_z)_z}{b_z}. \tag{15}$$

The expression for ψ at the channel–basin interface can be obtained by integrating (14) from the northern edge of the basin to the interface (as in NV11) to give

$$\psi|_{y^*} \approx -L_b\left(\kappa\frac{b_{zz}}{b_z} + \kappa_z\right). \tag{16}$$

The second term on the right-hand side that accounts for vertical variations in κ was not included in NV11, yet it is crucial for the discussion that follows.

The diffusive circulation in (16) must match the channel circulation given by (5) at $y = y^*$. This matching condition gives

$$K_e s_b \approx -L_b\left(\kappa\frac{b_{zz}}{b_z} + \kappa_z\right), \tag{17}$$

noting that the balance is valid only at the channel–basin interface. By introducing h as a characteristic vertical length scale for stratification, $H_{\rm mix}$ as the vertical decay scale of diapycnal mixing, l as the scale of meridional stratification in the channel, and κ_b as the value of the diffusivity at the ocean bottom, (17) can be reduced to an algebraic equation that may be employed to study the leading-order balance, namely,

$$\underbrace{-\frac{K_e h}{l}}_{\rm I} \propto -L_b\kappa_b\left(\underbrace{\frac{1}{h}}_{\rm II} - \underbrace{\frac{1}{H_{\rm mix}}}_{\rm III}\right). \tag{18}$$

Since I in (18) is always negative, only two limiting balances exist: (i) for $h \ll H_{\rm mix}$, I and II balance each other, and (ii) for $h \approx H_{\rm mix}$, the two terms on the right-hand side balance, with their residual being equal to the left-hand side (LHS). The term h is estimated to be $O(10^3)$ m in the real ocean, as we show below, assuming $h \ll H_{\rm mix}$ is equivalent to assuming no significant vertical variation in κ. Therefore, limit (i), considered for example by NV11 for the deep ocean, may be less relevant for the real ocean than limit (ii). Most importantly, limit (i) implies that the MOC is a weak residual of large terms, while limit (ii) predicts an MOC whose strength increases linearly with κ_b.

To put our results in the context of the real ocean, in Fig. 4a we plot globally averaged profiles of diapycnal diffusivity from an inverse model based on hydrographic sections (Lumpkin and Speer 2007) from a parameterization of the spatially variable diffusivity based on a large collection of microstructure data from several oceanic regions (Decloedt and Luther 2012, 2010) and from an estimate based on the calculation of internal waves radiated from bottom topography (Nikurashin and Ferrari 2013). In Fig. 4b, we plot the globally averaged $h \approx b_z/b_{zz}$ estimated from the World Ocean Circulation Experiment (WOCE) hydrography (Gouretski and Koltermann 2004). Together, the two panels show that the global stratification scale and the mixing decay scale are both in the range of 1000–1500 m. Notice that all the curves in the figure are global averages. The decay scale of mixing above individual topographic features may be shorter, but these average curves are the appropriate ones for a globally averaged perspective. A leading-order balance between the two terms on the RHS of the scaling relation (18) is also confirmed by substituting typical values representative of the present-day ocean (as listed in Table 1); the LHS term is at least an order of magnitude smaller than the RHS terms.

Assuming a balance between II and III in (18), we are led to expect that the buoyancy stratification increases on a scale

$$h_{\rm DL} \approx H_{\rm mix}. \tag{19}$$

In physical terms, the balance between II and III states that the diapycnal flux is constant in the vertical, that is, $\partial_z(\kappa b_z) \approx 0$, despite the decrease in κ. This is achieved by the stratification b_z increasing inversely with respect to the upward decrease in κ and leads to the formation of a weakly stratified region in the basin within which isopycnals intersect the bottom. Since the stratification in the channel must match that in the basin, the channel isopycnal slopes in the vicinity of the basin scale as $s_b = -b_y/b_z \approx H_{\rm mix}/l$. This mixing-induced steep slope drives a strong eddy-driven circulation of magnitude

$$\psi_{\rm DL} \approx -\frac{K_e H_{\rm mix}}{l}. \tag{20}$$

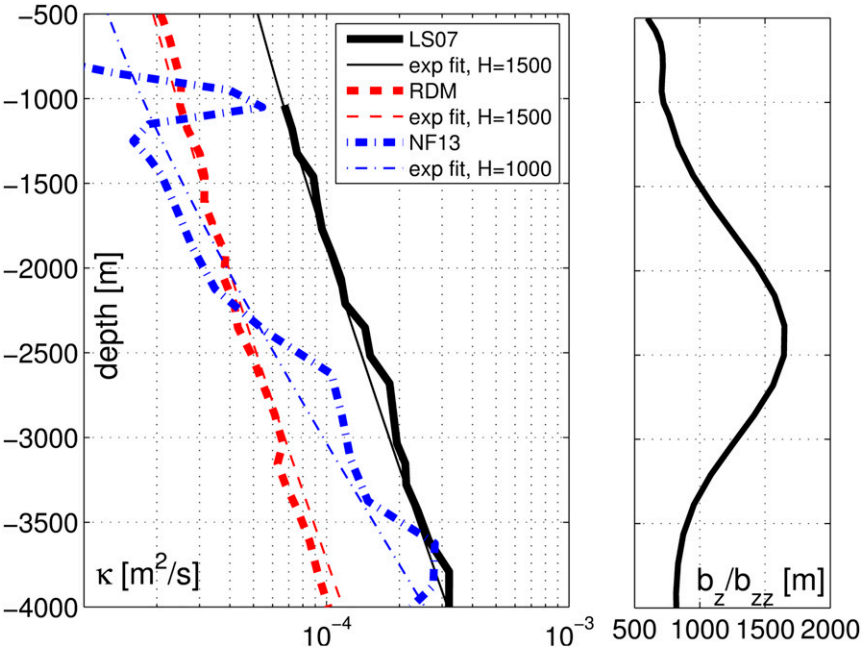

FIG. 4. Globally averaged (north of 55°S) diapycnal diffusivity profiles from Lumpkin and Speer (2007), Decloedt and Luther (2012), and Nikurashin and Ferrari (2013); indicated as LS07, RDM, and NF13, respectively in the legend. The thin line overlaying each diffusivity profile is an exponential fit using the vertical scale H shown in the legend; (b) globally averaged b_z/b_{zz} as the representative of abyssal stratification scale h, calculated from the WOCE dataset (Gouretski and Koltermann 2004). Both (a) and (b) share the same vertical axis.

Interestingly, (20) suggests that, to first order, the rate of the abyssal MOC depends on the mixing decay scale but not on the magnitude of the diapycnal diffusivity. It is important to note that a balance between I and II in (18), the limit explored in NV11, is also theoretically realizable. However, we choose to focus on the limit most relevant for the real ocean, which we showed above to be that in which II $\sim$ III.

Following (15) and (20), the upwelling velocity in the basin DL in this limit is

$$w_{\mathrm{DL}} \approx \frac{\psi_{\mathrm{DL}}}{L_b} \approx \frac{K_e s_b}{L_b} \approx K_e \frac{H_{\mathrm{mix}}}{l L_b}, \tag{21}$$

which is primarily set by channel eddies and basin mixing. This, however, is merely a scaling relation for the magnitude of w_{DL}. Equation (15) implies that $\partial_z(w_{\mathrm{DL}}) < 0$ since upwelling decreases upward as one tends to shallower depths in the upper layer where diabatic effects become smaller. In contrast, $\partial_z(w_{\mathrm{ABL}}) \approx \partial_z(\psi_{\mathrm{ABL}}/L_b) > 0$ because of the upward increase in vertical velocity from zero at the bottom boundary. We will show that the change in sign of w_z across the ABL–DL boundary is dynamically linked to the northward flow in the ABL and southward flow in the DL.

e. *The ocean basin: The upper adiabatic layer*

This limit has been discussed in detail in Marshall and Radko (2006), Wolfe and Cessi (2010), Wolfe and Cessi (2011), and NV11 and is relevant for the upper ocean where diapycnal mixing is considerably smaller than in the abyssal and deep layers; hence, it is referred to as adiabatic. Waters at these depths are usually referred to as intermediate. While these waters form the topmost layer in our setup, it is important to note that in the real ocean intermediate waters lie below the wind-driven gyres.

In the limit of small diapycnal mixing, (14) implies that the circulation must be weak. NV11 conclude that

TABLE 1. Parameter ranges relevant to the real ocean. The quantity ψ in this table corresponds to the estimates of AABW circulation in the abyssal and deep layers close the channel–basin interface (Lumpkin and Speer 2007; Ganachaud 2003).

ψ_{DL}	0.01–0.1 ($\mathrm{m^2\,s^{-2}}$) $\approx$ 0.1–1 (Sv)
ψ_{ABL}	0.1–1 ($\mathrm{m^2\,s^{-2}}$) $\approx$ 1–10 (Sv)
H_{mix}	10^2–10^3 (m)
κ_b	10^{-4}–10^{-3} ($\mathrm{m^2\,s^{-1}}$)
K_e	10^3 ($\mathrm{m^2\,s^{-1}}$)
L_b	10^7 (m)
$l \approx L_c$	10^6 (m)

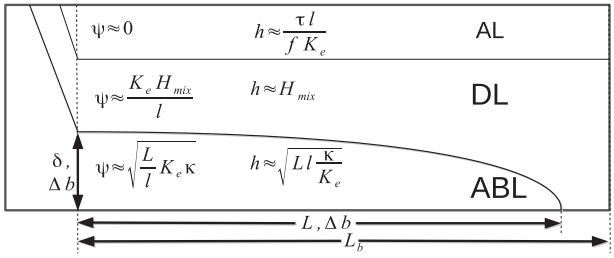

FIG. 5. Schematic summary of the scaling relations.

at leading order the wind and eddies balance so as to result in a small MOC as per (3): $\psi = \tau/f\rho_0 + K_e s_b \simeq 0$. Thus, channel isopycnal slopes are set by surface winds and eddies through

$$s_b \approx -\frac{\tau}{K_e f \rho_0}. \tag{22}$$

In this limit, isopycnals enter into the ocean at a slope s_b in the channel and become flat at the channel–basin interface. The circulation consists of a weak along-isopycnal flow in the channel and a weak diffusive flow that crosses isopycnals in the basin.

f. Summary of the scaling relations

To summarize, the vertical variation in mixing leads to a layered basin structure consisting of a bottom abyssal boundary layer (ABL), a deep layer (DL), and an upper adiabatic layer (AL) that represents the circulation of abyssal, deep, and intermediate water masses, respectively. The three layers are summarized schematically in Fig. 5. In the ABL, diapycnal mixing in the basin and eddies in the channel set the circulation and stratification, with the vertical structure of mixing playing a secondary role. In the DL, mixing in the basin (especially its vertical structure) and eddies in the channel together set the stratification and rate of circulation. In the AL, the stratification in the basin is primarily set by the winds and eddies acting on the channel and setting the isopycnal slopes there. The scaling relation used for h in the top layer in the figure may be easily derived from (22).

3. Numerical tests with an ocean circulation model

a. Numerical experiment setup

In the previous section, we presented qualitative scaling arguments for the abyssal MOC and stratification in a zonally averaged sense. The scaling relationships are now tested with 3D numerical solutions of the governing equations obtained by running an ocean general circulation model.

We use the Massachusetts Institute of Technology general circulation model (MITgcm; Marshall et al. 1997). The model setup includes a single basin bounded by vertical walls at the northern and lateral boundaries. The basin is connected to a reentrant channel to the south, as shown in the top panel of Fig. 6. The horizontal resolution is 2° × 2°. The domain extends over 130° of longitude and from 60°S to 60°N for a total basin surface area similar to that of the Pacific Ocean. There are no lateral boundaries between 60° and 40°S, and the flow in this range is zonally periodic. Because of the coarse resolution in our model, the effect of eddies is parameterized with the Gent and McWilliams (1990) scheme. The bottom topography is flat. The model is configured with 40 vertical levels with thicknesses stretching from 10 m at the top to 270 m at the bottom. Therefore, the bottom weakly stratified layer in which isopycnals bend downward and intersect the bottom at a normal angle will not be fully resolved, especially for cases with smaller κ_b, as will be clear in Figs. 7 and 9 (shown below).

The model is forced over the topmost grid cell by restoring temperature to a prescribed profile on a time scale of a month. The restoring temperature profile is zonally uniform and increases with latitude from the south up to the equator (see Fig. 6, bottom panel). We use a linear equation of state and set salinity to a constant; thus, temperature is the sole contributor to buoyancy. A zonally uniform wind stress (shown in Fig. 6) blows only over the channel; the stress peaks at $0.2\,\mathrm{N\,m^{-2}}$ in the center of the channel and decays toward the north and south channel boundaries. The choice to apply winds only at the channel is made to cleanly separate the stratification and MOC impacts of southern channel winds and eddies from the enhanced abyssal mixing in the basin. Wind-driven basin gyres are not expected to have a leading-order influence on the deep-ocean dynamics and so are omitted in the simulations. Similarly, the geothermal heat flux through the ocean floor has been known to affect the MOC (Mashayek et al. 2013; Lavergne et al. 2015, manuscript submitted to *J. Phys. Oceanogr.*), but it is expected to change, only in a minor quantitative way, the results presented herein. Similar experimental setups have been employed in the literature to study the role of Southern Ocean dynamics on the meridional overturning circulation and deep stratification (e.g., Viebahn and Eden 2010; Morrison et al. 2011; NV11; Munday et al. 2013).

The mixing profile is set through a horizontally uniform diapycnal diffusivity that increases toward the ocean bottom:

$$\kappa(z) = \kappa_t + (\kappa_b - \kappa_t) e^{(z+D)/H_{\mathrm{mix}}}, \tag{23}$$

where κ_t is a background diffusivity set to $1 \times 10^{-5}\,\mathrm{m^2\,s^{-1}}$, κ_b is the bottom diffusivity, H_{mix} is the

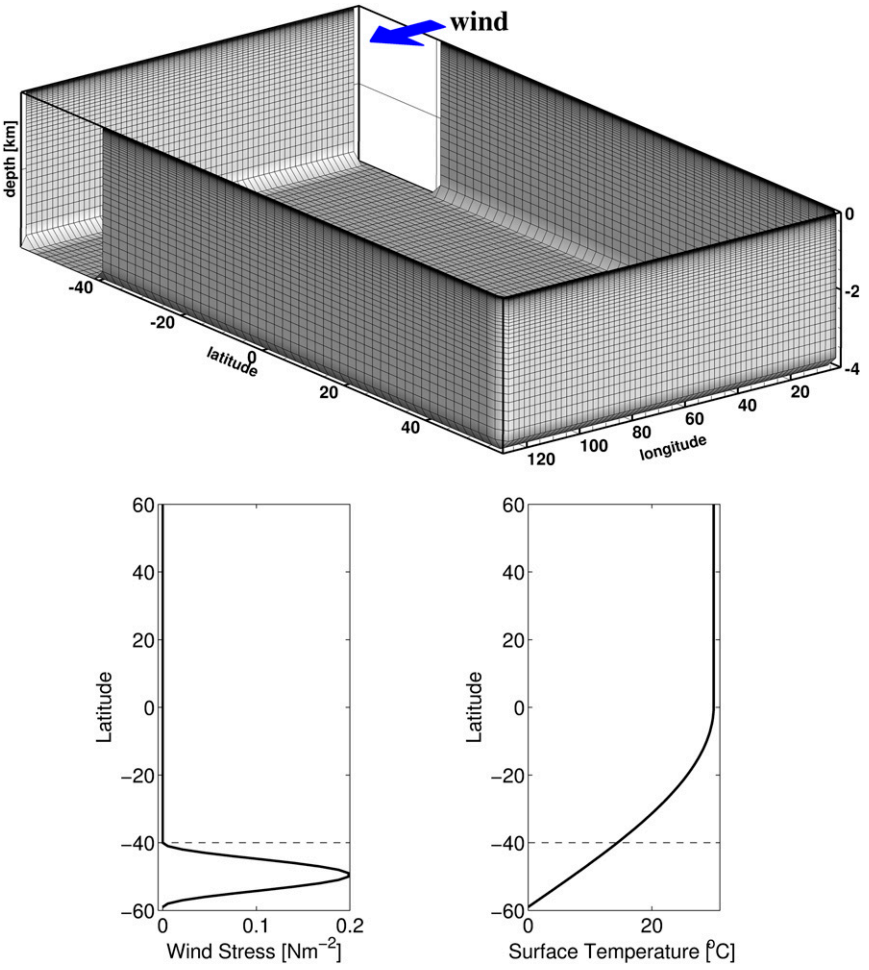

FIG. 6. (top) Computational domain; (bottom) zonally uniform wind profile and surface temperature employed in the model.

mixing decay scale, and D is the ocean depth set to 4000 m. A suite of numerical tests with different values of κ_b and $H_{\rm mix}$ are performed to verify the scaling relations derived in section 2. In most simulations, we use a constant lateral eddy diffusivity K_e set to $1000\,{\rm m^2\,s^{-1}}$, but a few test cases will also be presented in which K_e is varied between 500 and $1500\,{\rm m^2\,s^{-1}}$. The simulations are run until a steady state is achieved, that is, until the change in the meridional overturning streamfunction at the channel–basin interface is smaller than 5% over 1000 yr.

b. Description of the numerical solutions

In Fig. 7, we compare results from three simulations using different values of κ_b; all three cases share the same values of $\kappa_t = 10^{-5}\,{\rm m^2\,s^{-1}}$ and $H_{\rm mix} = 500$ m, while κ_b values increase from the top to the bottom panels. Right panels in the figure show the basin-averaged stratification b_z alongside an exponential fit with decay scale of $H_{\rm mix}$. In all three cases a well-defined ABL develops above the ocean floor. However, $\kappa_b \approx \kappa_t$ for a κ with weak vertical variation (top row); the ABL is confined to just a few grid points at the bottom of the domain. The ABL becomes thicker when $\kappa_b \gg \kappa_t$, and thus κ is enhanced at depth (two bottom panels). Above the ABL, a strongly stratified DL develops, where the stratification increases upward inversely with the decay in κ as shown in the right panels of the figure and consistent with our argument that $\partial_z(\kappa b_z) \approx 0$ (right panels). It is in this layer that the exponential fit to the stratification is most accurate. On top of the DL lies the AL, where the stratification is set by wind and eddies in the channel through (22) and the assumption that isopycnals flatten in the basin holds. The MOC becomes stronger and more bottom intensified for the simulations with a larger value of κ at the bottom.

At this point, it is instructive to test the validity of the assumptions made with respect to the dominant balances in the momentum and buoyancy budgets used in the discussion leading to relation (17). To do so, in Fig. 8

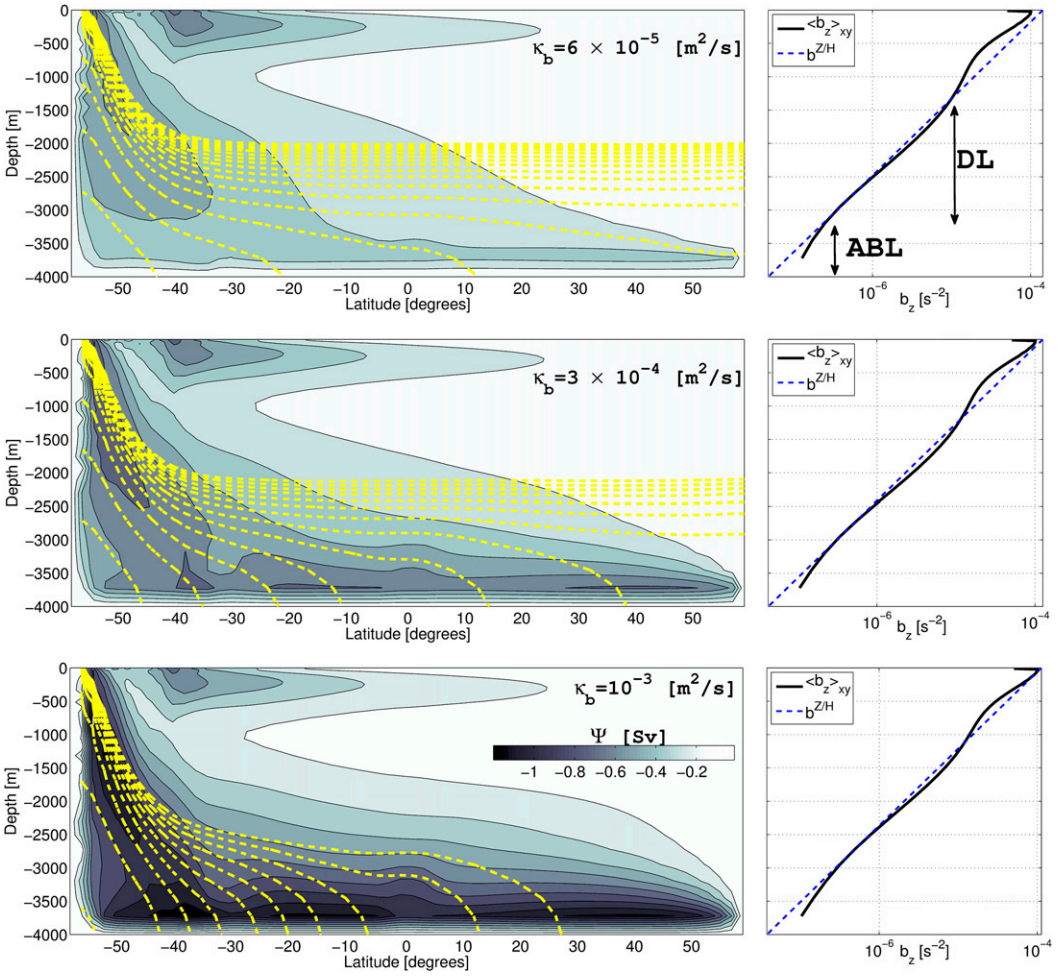

FIG. 7. Sensitivity of MOC and stratification to enhancement of abyssal mixing. The term κ_b increases from the top to bottom with $H_{\rm mix} = 500$ m for all cases. (left) Contour of zonally integrated meridional overturning streamfunction overlaid by isopycnals in the deep ocean. Isopycnals are only plotted in the deep ocean to avoid cluttering the plots in the top 2000 m; (right) basin-averaged stratification b_z plotted against an exponential fit with decay scale of $H = H_{\rm mix}$. The depth range over which the two curves agree corresponds to the DL where $\partial_z(\kappa b_z) \approx 0$.

we plot various terms in (17), all at the channel–basin interface and normalized by the wind-induced circulation in the channel, for the simulation shown in the middle panel of Fig. 7. Below the depth of 2000 m, the three terms kept in (17) do in fact dominate the wind circulation, thereby justifying dropping $\overline{\psi}$ from the balance. Furthermore, the figure clearly shows that the two terms on the RHS of (17) are indeed larger than the eddy-induced term by an order of magnitude, with their residual balanced by the eddy circulation in the channel. The balance between the terms on the RHS implies $h \sim H_{\rm mix}$, as given by scaling relation (19) and consistent with the right panel of the middle row in Fig. 7.

In Fig. 9, we show the impact of changing the vertical scale over which κ is enhanced $H_{\rm mix}$. In the DL, the leading-order balance for $H_{\rm mix} \ll D$ is $\partial_z(\kappa b_z) \approx 0$, that is, a balance between II and III in (18). However, as $H_{\rm mix}$ approaches D, starting from $H_{\rm mix} = 750$ m, the balance in (18) shifts to I $\sim$ II, which is the constant diffusivity limit discussed in NV11. Furthermore, as we move from sharp (top) to mild (bottom) vertical variations in mixing, the circulation becomes stronger because of the diminishing cancellation between the two terms on the RHS of (16). A similar sensitivity to $H_{\rm mix}$ was reported by Saenko et al. (2012) using a global general circulation model.

c. *Verification of scaling relations*

Next, we use the numerical simulations to quantitatively test the scaling relations introduced in section 2. In Fig. 10, we plot the overturning streamfunction and stratification scale diagnosed from model outputs. Both

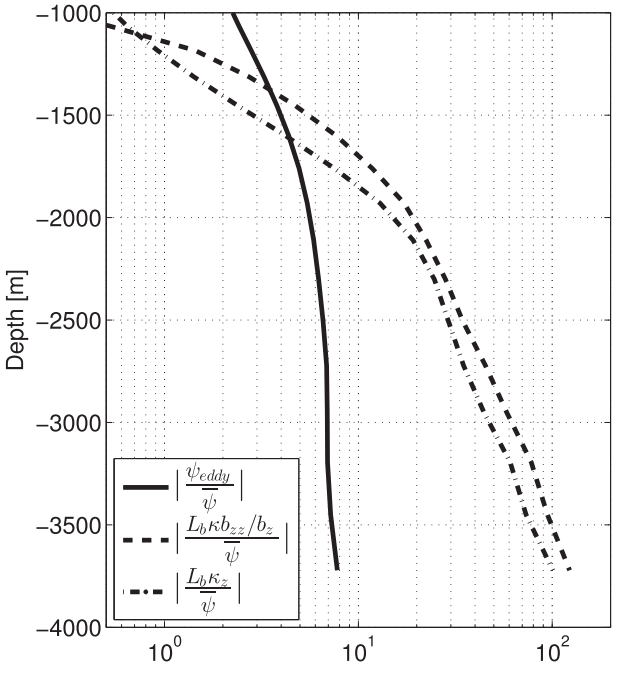

FIG. 8. Plot of the terms in (17), all at the channel–basin interface and normalized by the wind-induced circulation in the channel for the simulation shown in the middle panel of Fig. 7.

ψ and h are measured at the location of the maximum in ψ at the channel–basin interface (40°S). The stratification scale is estimated as $h \approx b_z/b_{zz}$. (A separate method of estimating h by fitting exponential profiles to b led to similar results.) The symbols on the plot are color coded with red representing shallower depths (for the location of the maximum) and blue representing deeper depths. The two panels in the left column show diagnosed ψ_{peak} and h_{peak} normalized by DL scaling relations (20) and (19), while the panels on the right show ψ_{peak} and h_{peak} normalized by ABL scaling relations (13) and (12). In the small κ limit, the MOC lies completely within the DL (red symbols) and ψ_{peak} and h_{peak} scale nicely with the DL scaling relations. For larger κ_b, the peak of the MOC moves deeper. In the large κ limit, the peak lies in the ABL close to its upper boundary, implying a northward flow in the ABL and a return flow in the DL. Both ψ_{peak} and h_{peak} scale nicely with the ABL scaling relations, as is shown in the right panels.

It is important to point out that although Fig. 10 shows ψ and h measured only at the peak of the MOC, when they are averaged separately over DL and ABL, the agreement with the corresponding scalings for each layer is strong (not shown). Variations in the horizontal scale of the stratification L can be ignored because they do not exceed a factor of 2, much smaller than the variations of κ_b, but are responsible for the scatter between the scaling relations and the simulation results.

Figure 11 shows that the scaling relations for the ABL and DL hold well when K_e is changed over a range of values from 500 to 1500 $\text{m}^2\,\text{s}^{-1}$. We do not mean to suggest a certain dependence of MOC strength on K_e, since the latter is itself a function of other flow parameters like the winds and κ. This figure is meant simply to provide a consistency check between our numerical simulations and theoretical scaling relations for cases in which K_e is prescribed.

d. The 3D abyssal circulation

While the zonally averaged perspective upon which we have focused to this point is helpful in quantifying the basic characteristics of the MOC, there are important aspects of the full 3D circulation that require a separate perspective. For this reason we have analyzed the full 3D circulation of a reference case run with a profile of κ with $\kappa_b = 3 \times 10^{-4}\,\text{m}^2\,\text{s}^{-1}$ and $H_{\text{mix}} = 500\,\text{m}$, values representative of the profiles measured in the present-day oceans as per Fig. 4. This is the simulation used to produce the middle panel of Fig. 9 as well as Fig. 8.

In Fig. 12, we show contours of the horizontal quasi streamfunction[3] (left column; see figure caption for definition) as well as streamlines (right column) at various depth levels. There is a strong northward (blue) flow in the ABL below $z \sim -3500\,\text{m}$ and a weaker southward flow in the DL between −3500 and −2500 m. The circulation in both layers is characterized by planetary gyres driven by the vortex stretching associated with vertical mixing (Stommel and Arons 1960).[4] To analyze the gyres more quantitatively, we note that the vorticity budget in the basin is (see appendix for derivation)

$$fw_z^* + \mathcal{T}_e = \beta v^*, \tag{24}$$

where velocities are residual (indicated by the star) and where $\mathcal{T}_e$ is the curl of the eddy stress contributions (see appendix for definition). Equation (24) is an extension of the balance of Stommel and Arons (1960) that accounts for the effect of mesoscale eddies. In what follows we show that the balance between the three terms in (24) changes from the ABL to the DL in such a way as to imply northward flow in the ABL and a southward

[3] The term "quasi" is employed since the horizontal velocity integrated to obtain the plotted streamfunction contours is not divergenceless.

[4] Notice that the strong gyre near the ocean surface north of the channel (visible in the last panel of Fig. 12) is driven by the meridional buoyancy gradient imposed over the Southern Hemisphere. This cell could easily be avoided had the surface density gradient been limited to the channel latitude band.

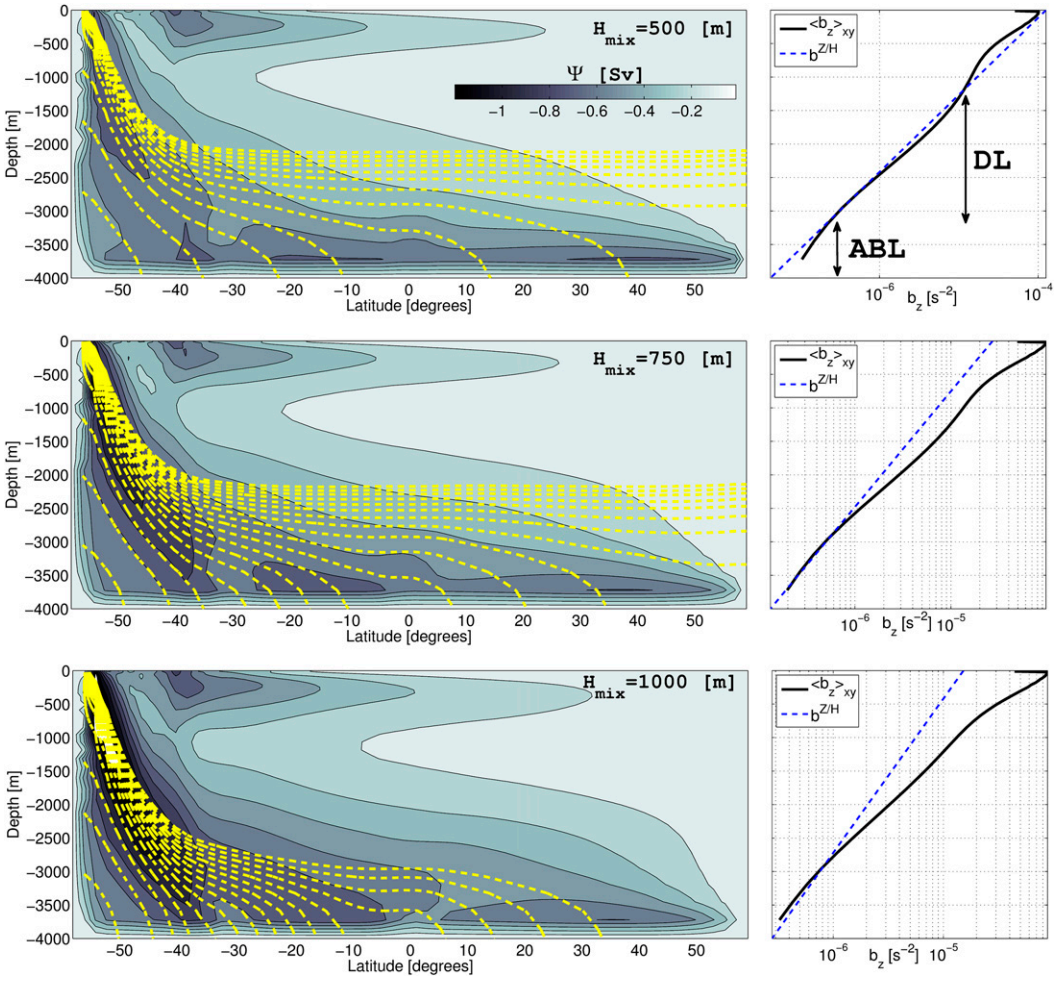

FIG. 9. As in Fig. 7, but for the sensitivity of MOC to vertical decay scale H_{mix}. The diffusivity $\kappa_b = 3 \times 10^{-4}\,\mathrm{m^2\,s^{-1}}$ for all three cases, while H_{mix} changes from 500 m (top) to 1000 m (bottom). Note that the top panel is the same as the middle panel in Fig. 7.

horizontal return flow in the DL, thereby enabling closure of the MOC. We do so by showing the integrals of three terms in (24) in Fig. 13 for the Southern Hemisphere basin (left), Northern Hemisphere (middle), and entire basin (right). The western boundary currents are excluded from the horizontal integrals because (24) is not expected to hold in the inertial and frictional boundary layers. Therefore, the following discussion is focused on horizontal transport by the interior gyres alone. To relate the horizontal gyre circulations to the zonally averaged circulation discussed in previous sections, one will need to account for the combined transport in gyres as well as in boundary currents, as we will briefly discuss at the end of this section.

In the ABL, the eddy stress term $\mathcal{T}_e$ is leading order since the isopycnal slope is large (Fig. 13). In the Southern Hemisphere ABL, the vortex squeezing fw^* and eddy stresses $\mathcal{T}_e$ together facilitate a northward meridional flow. In the northern ABL, mixing-induced vortex stretching, albeit partially offset by the eddy stresses, results in a northward transport. Thus, the net interhemispheric flow due to gyres in the ABL is northward.

In the DL, all terms in (24) are smaller, and hence the associated gyres are much weaker. In the Southern Hemisphere DL and for depths shallower than 2500 m, eddy stresses dominate (and cancel) the vortex stretching effect, resulting in a southward flow. Thus, the sense of circulation cannot be inferred from the vortex stretching alone. In the Northern Hemisphere DL, an upward decay in upwelling velocity is associated with a southward flow. Thus, the net interhemispheric flow due to gyres in the DL is southward.

The budget in (24) differs in an important conceptual way from the classical work of Stommel and Arons (1960). The vorticity budget is computed using residual velocities, that is, the velocities that advect

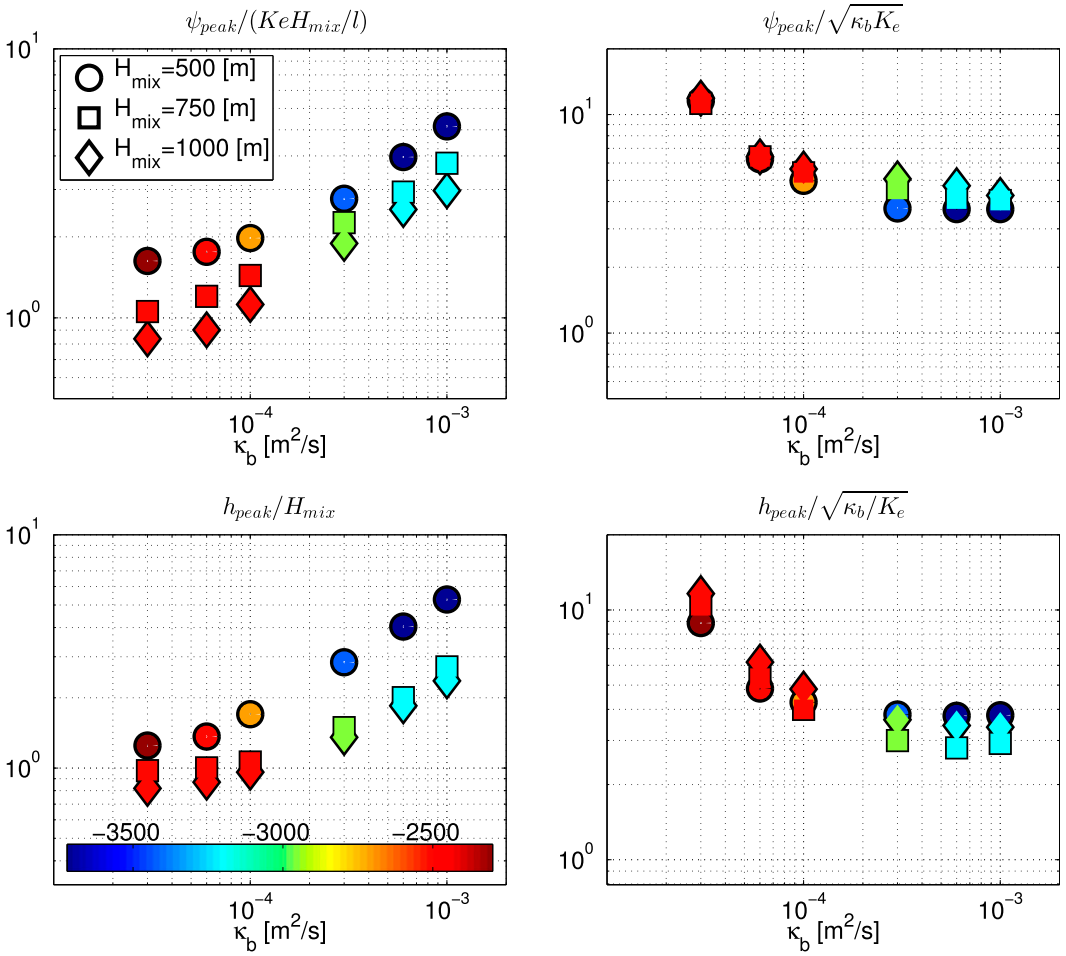

FIG. 10. Plots of the rate of overturning circulation and the stratification scale diagnosed from simulations at different values of κ_b and H_{mix}. The terms ψ and h are measured at the location of the peak of the overturning streamfunction and at the channel–basin interface (40°S). The symbol colors represent the depth of the location of the peak with red and blue representing shallower and deeper, respectively. (left) Diagnosed ψ_{peak} and h_{peak} normalized by DL scaling relations for ψ_{DL} and h_{DL} proposed in (20) and (19); (right) ψ_{peak} and h_{peak} normalized by ψ_{ABL} and h_{ABL} given in (13) and (12).

tracers like PV. It is the residual velocities that achieve the squeezing and stretching of the planetary vorticity. By working in terms of residual velocities, the effect of eddies appears explicitly in the vorticity budget [(24)].

The western boundary currents were not included in integration of the various terms plotted in Fig. 13, but they play an important role in closing the abyssal meridional overturning circulation. This is shown in the right panels of Fig. 12 that illustrate important vertical and horizontal transports within the boundary currents. Our focus in this section was upon determining the dominant balance governing the basinwide gyre circulation at various ocean depths. A detailed discussion of vertical and horizontal transports within the boundary currents is beyond the scope of this idealized study and would at the very least require simulations with more realistic bottom topography.

4. Conclusions

We have investigated the impact of the sharp increase in mixing rates at the ocean bottom on the abyssal stratification and circulation of an idealized ocean. To make analytical progress, we considered a simple geometry composed of a reentrant channel connected to a closed basin to the north. The enhancement of mixing was imposed through a vertical profile of diapycnal diffusivity that increased exponentially with depth. The idealized ocean was forced with winds and buoyancy forcing along the channel, while no wind forcing was imposed on the basin. In this configuration, dense waters

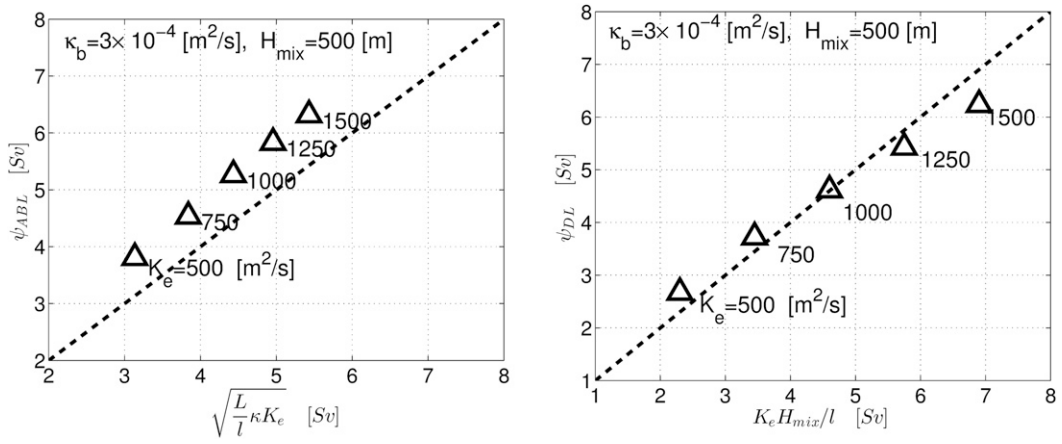

FIG. 11. Verification of the predicted sensitivity of scaling relations (20) and (13) to eddy diffusivity. The value of L is set to L_b in the construction of the left panel.

formed only in the channel and flowed into the basin along the bottom, a situation analogous to that found in the Indian and Pacific Oceans.

The enhancement in diapycnal diffusivity resulted in solutions characterized by different dynamics as a function of depth. An abyssal boundary layer formed at the bottom, where mixing was most intense, the stratification was weak and the circulation flowed horizontally from the channel into the basin. The isopycnals curved so as to intersect the ocean bottom at right angles and satisfy the no buoyancy flux boundary condition. We found the thickness of this layer to be set by the vertical decay scale of mixing. We believe that this layer describes the circulation of abyssal waters in the real ocean. A second layer developed above the abyssal boundary layer characterized by flat isopycnals and a weak circulation in the basin that brought waters upward from the abyssal layer and back into the channel. The stratification increased inversely proportional to the diapycnal diffusivity κ, resulting in a small diapycnal flux (given by the product of κ and the stratification.) In stark contrast to previous studies that ignored variations in abyssal mixing, the circulation strength was found to be proportional to the vertical scale over which mixing decreases but not on its magnitude (The circulation is instead proportional to the mixing magnitude in the abyssal boundary layer.) Given that the vertical profile of mixing is largely set by the distribution of topographic features at the ocean bottom, this study highlights the important role played by these features in setting the global abyssal stratification and circulation. This layer appears to correspond to the circulation of deep waters in the real ocean. Finally, a third layer developed above the other two, where mixing was weak and did not affect the dynamics. This layer corresponds to the circulation of intermediate waters in the real ocean and has been the focus of numerous recent studies (e.g., Wolfe and Cessi 2010; NV11).

We derived scaling laws for the circulation and stratification in these three layers, which were then verified with three-dimensional numerical simulations. Most importantly, we showed that the solutions undergo an important transition when the diapycnal diffusivity varied little in the vertical. In this limit, the abyssal bottom layer became very thin and the two top layers merged into one. The overturning circulation was then found to be proportional to the diapycnal diffusivity, while the stratification was not. Indeed as the diapycnal diffusivity was increased, the stratification changed little, while the circulation increased: a response opposite to the limit where the diapycnal diffusivity increased rapidly toward the bottom. Using ocean estimates of diapycnal diffusivity, we confirmed that the limit of strong variations in vertical mixing and three-layered structure is more relevant for the real ocean.

Our results brought to the fore an interesting conundrum. Despite the prescribed increase in diapycnal diffusivity toward the bottom, the diapycnal flux decreases with depth. This is consistent with an overturning circulation with abyssal waters rising in the basins, as observed in the real ocean (e.g., Lumpkin and Speer 2007). In a zonally averaged sense, the buoyancy budget in the ocean basins above the abyssal boundary layer is given by a balance between the vertical advection and the downward diffusion of buoyancy $\psi b_z \sim \partial_z(\kappa b_z)$, where ψ is the overturning streamfunction. This balance requires that for an anticlockwise circulation to exist in the abyss (as observed in the real ocean), κb_z must increase with height. The conundrum is that observations typically report diapycnal fluxes that increase

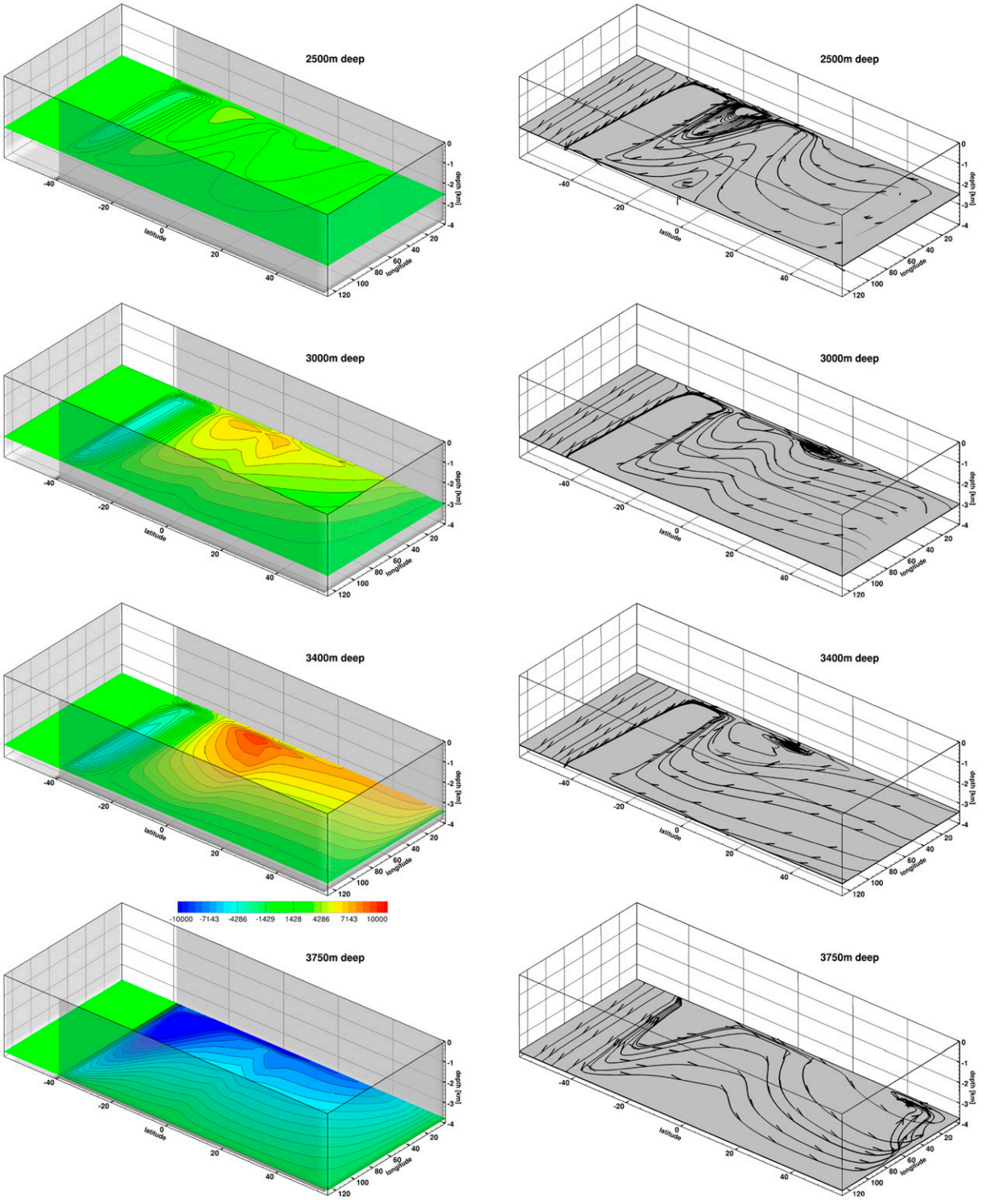

FIG. 12. (left) Horizontal circulation streamfunction ($m^2\,s^{-1}$) and (right) corresponding streamlines plotted at various depths. The streamfunction is defined as $\phi = \int_{x_E}^{x} v\,dx$, where x_E represents the eastern boundary. Blue and red represent northward and southward flows, respectively. The streamfunction in the channel is not shown. The depth level 3550 m (not shown) represents the approximate boundary between the northward flow in the ABL and the southward return flow in the DL. All plots are for the same case as that shown in the top panel of Fig. 9.

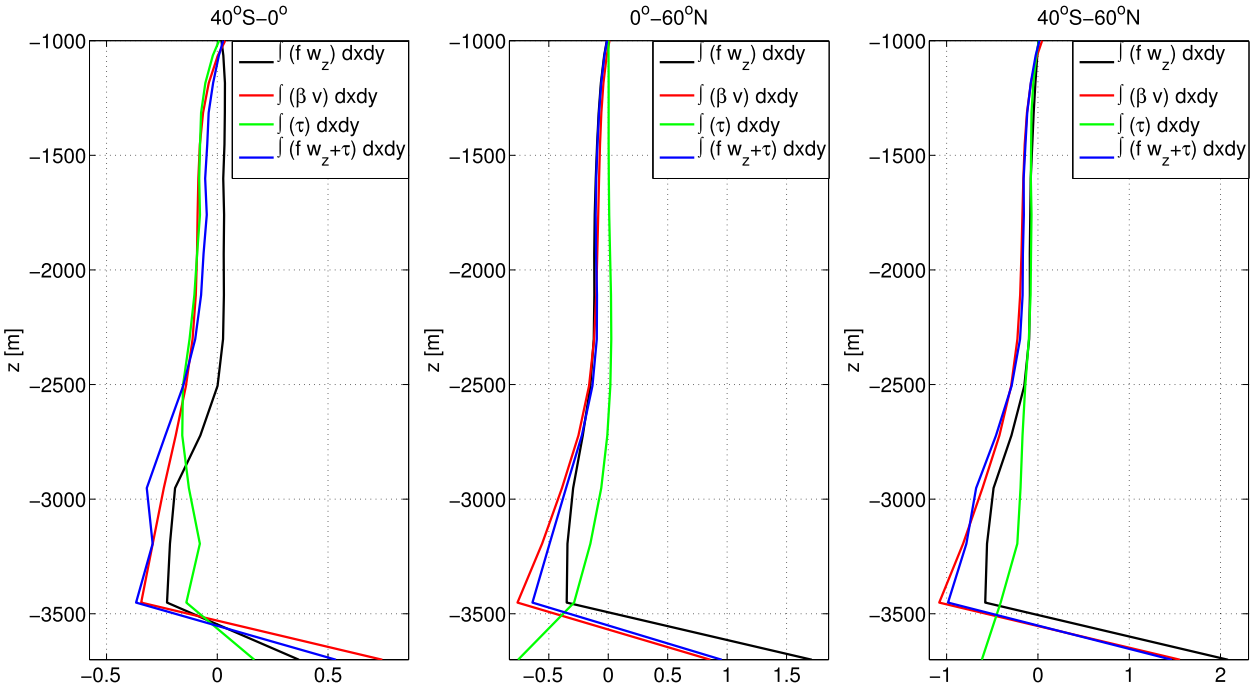

FIG. 13. Integrals of various components of (24) diagnosed from the simulation shown in Fig. 12. All components are integrated horizontally (left) over the Southern Hemisphere (excluding the channel), (middle) over the Northern Hemisphere, and (right) over the entire basin (again excluding the channel). All integrals exclude the western boundary current. The unit for all curves is $m^2 s^{-2}$. Note that the close proximity of the red and blue curves indicates satisfactory closing of the vorticity budget [(24)].

with depth (e.g., Waterhouse et al. 2014). We speculate that the complex nature of spatial variations of diapycnal mixing may result in vertical profiles of the basin-averaged fluxes that are different from individual profiles. Reconciling the vertical structure of diapycnal mixing with the observed meridional overturning circulation is the topic of an upcoming paper.

Another outcome of our analysis is that the zonally averaged perspective on the meridional circulation misses important aspects of the impact of variable vertical mixing on the full three-dimensional circulation. We found that in response to the mixing variations, the vertical velocities increase rapidly from zero to finite values through the abyssal layer, resulting in a vortex stretching contribution that spins up a vigorous gyre circulation much like that surmised in the classical work of Stommel and Arons (1960). The gyre circulation is, however, much weaker in the deep layer where the vertical velocities are relatively constant.

Finally, it should be acknowledged that our results apply to a very idealized geometry. Future work will be needed to verify to what extent our arguments can be extended to the more complex geometry of the real ocean. In particular, the circulation and scaling of the abyssal bottom layer are likely to be modified by the presence of a corrugated topography punctuated by ridges and rises. Sloping boundaries may also be important in the dynamics of the two upper layers. We are, however, confident that the three-layered structure of the circulation and stratification that results from vertical variations in mixing is an important aspect of ocean dynamics, and hopefully it will help in the interpretation of the flows that characterize the abyssal, deep, and intermediate water masses of the real ocean.

Acknowledgments. A. M. and R. F. acknowledge NSF support through Award OCE-1233832. A. M. also acknowledges support from an NSERC postdoctoral fellowship. We wish to thank L. P. Nadeau for help with implementation of the numerical model as well as for many helpful comments on the manuscript. We also wish to thank T. Decloedt and K. Speer for providing the data for diffusivity profiles employed in the production of Fig. 4.

APPENDIX

Derivation of the Vorticity Budget (A4)

Following Plumb (1986), the residual momentum balance in the basin in the absence of any surface wind forcing and in the limit of small Rossby number is

$$-f\upsilon^* = -\frac{1}{\rho_0}p_x + f\partial_z\tau_e^x, \quad \text{and} \tag{A1}$$

$$fu^* = -\frac{1}{\rho_0}p_y + f\partial_z\tau_e^y, \tag{A2}$$

where velocities are residual (indicated by the star). Eddy stresses τ_e^x and τ_e^y are defined as

$$\tau_e^x = \frac{\overline{\upsilon' b'}}{\overline{b}_z}, \quad \tau_e^y = -\frac{\overline{u' b'}}{\overline{b}_z}, \tag{A3}$$

where primes denote eddy properties and bars denote averaging over many eddy scales, which in our case is temporal. In our model, τ_e^x and τ_e^y are parameterized in the form of $\tau_e^x = -K_e\overline{b}_y/\overline{b}_z$ and $\tau_e^y = K_e\overline{b}_x/\overline{b}_z$. Equations (A1) and (A2) can be cross differentiated and subtracted from each other to give the vorticity budget

$$fw_z^* + \mathcal{T}_e = \beta\upsilon^*, \tag{A4}$$

where the continuity equation has been used and where

$$\mathcal{T}_e = f\partial_z(\partial_x\tau_e^y - \partial_y\tau_e^x) - \beta\partial_z\tau_e^x. \tag{A5}$$

REFERENCES

Andrews, D., and M. McIntyre, 1976: Planetary waves in horizontal and vertical shear: The generalized Eliassen-Palm relation and the mean zonal acceleration. *J. Atmos. Sci.*, **33**, 2031–2048, doi:10.1175/1520-0469(1976)033<2031:PWIHAV>2.0.CO;2.

Decloedt, T., and D. S. Luther, 2010: On a simple empirical parameterization of topography-catalyzed diapycnal mixing in the abyssal ocean. *J. Phys. Oceanogr.*, **40**, 487–508, doi:10.1175/2009JPO4275.1.

——, and ——, 2012: Spatially heterogeneous diapycnal mixing in the abyssal ocean: A comparison of two parameterizations to observations. *J. Geophys. Res.*, **117**, C11025, doi:10.1029/2012JC008304.

Ganachaud, A., 2003: Large-scale mass transports, water mass formation, and diffusivities estimated from World Ocean Circulation Experiment (WOCE) hydrographic data. *J. Geophys. Res.*, **108**, 3213, doi:10.1029/2002JC001565.

Gent, P. R., and J. C. McWilliams, 1990: Isopycnal mixing in ocean circulation models. *J. Phys. Oceanogr.*, **20**, 150–155, doi:10.1175/1520-0485(1990)020<0150:IMIOCM>2.0.CO;2.

Gouretski, V., and K. Koltermann, 2004: WOCE global hydrographic climatology. Berichte des Bundesamtes für Seeschifffahrt und Hydrographie 35, 52 pp.

Ito, T., and J. Marshall, 2008: Control of lower-limb overturning circulation in the Southern Ocean by diapycnal mixing and mesoscale eddy transfer. *J. Phys. Oceanogr.*, **38**, 2832–2845, doi:10.1175/2008JPO3878.1.

Lumpkin, R., and K. Speer, 2007: Global ocean meridional overturning. *J. Phys. Oceanogr.*, **37**, 2550–2562, doi:10.1175/JPO3130.1.

Lund, D. C., J. F. Adkins, and R. Ferrari, 2011: Abyssal Atlantic circulation during the Last Glacial Maximum: Constraining the ratio between transport and vertical mixing. *Paleoceanography*, **26**, PA1213, doi:10.1029/2010PA001938.

Marshall, J., and T. Radko, 2003: Residual-mean solutions for the Antarctic Circumpolar Current and its associated overturning circulation. *J. Phys. Oceanogr.*, **33**, 2341–2354, doi:10.1175/1520-0485(2003)033<2341:RSFTAC>2.0.CO;2.

——, and ——, 2006: A model of the upper branch of the meridional overturning of the Southern Ocean. *Prog. Oceanogr.*, **70**, 331–345, doi:10.1016/j.pocean.2006.07.004.

——, A. Adcroft, C. Hill, L. Perelman, and C. Heisey, 1997: A finite-volume, incompressible Navier Stokes model for studies of the ocean on parallel computers. *J. Geophys. Res.*, **102**, 5753–5766, doi:10.1029/96JC02775.

Mashayek, A., R. Ferrari, G. Vettoretti, and W. Peltier, 2013: The role of the geothermal heat flux in driving the abyssal ocean circulation. *Geophys. Res. Lett.*, **40**, 3144–3149, doi:10.1002/grl.50640.

Melet, A., R. Hallberg, S. Legg, and K. Polzin, 2013: Sensitivity of the ocean state to the vertical distribution of internal-tide-driven mixing. *J. Phys. Oceanogr.*, **43**, 602–615, doi:10.1175/JPO-D-12-055.1.

Morrison, A. K., A. M. Hogg, and M. L. Ward, 2011: Sensitivity of the Southern Ocean overturning circulation to surface buoyancy forcing. *Geophys. Res. Lett.*, **38**, L14602, doi:10.1029/2011GL048031.

Munday, D. R., H. L. Johnson, and D. P. Marshall, 2013: Eddy saturation of equilibrated circumpolar currents. *J. Phys. Oceanogr.*, **43**, 507–532, doi:10.1175/JPO-D-12-095.1.

Munk, W., and C. Wunsch, 1998: Abyssal recipes II: Energetics of tidal and wind mixing. *Deep-Sea Res. I*, **45**, 1977–2010, doi:10.1016/S0967-0637(98)00070-3.

Nikurashin, M., and R. Ferrari, 2010a: Radiation and dissipation of internal waves generated by geostrophic motions impinging on small-scale topography: Application to the Southern Ocean. *J. Phys. Oceanogr.*, **40**, 2025–2042, doi:10.1175/2010JPO4315.1.

——, and ——, 2010b: Radiation and dissipation of internal waves generated by geostrophic motions impinging on small-scale topography: Theory. *J. Phys. Oceanogr.*, **40**, 1055–1074, doi:10.1175/2009JPO4199.1.

——, and G. Vallis, 2011: A theory of deep stratification and overturning circulation in the ocean. *J. Phys. Oceanogr.*, **41**, 485–502, doi:10.1175/2010JPO4529.1.

——, and R. Ferrari, 2013: Overturning circulation driven by breaking internal waves in the deep ocean. *Geophys. Res. Lett.*, **40**, 3133–3137, doi:10.1002/grl.50542.

Plumb, R. A., 1986: Three-dimensional propagation of transient quasi-geostrophic eddies and its relationship with the eddy forcing of the time-mean flow. *J. Atmos. Sci.*, **43**, 1657–1678, doi:10.1175/1520-0469(1986)043<1657:TDPOTQ>2.0.CO;2.

——, and R. Ferrari, 2005: Transformed Eulerian-mean theory. Part I: Nonquasigeostrophic theory for eddies on a zonal mean flow. *J. Phys. Oceanogr.*, **35**, 165–174, doi:10.1175/JPO-2669.1.

Saenko, O. A., X. Zhai, W. J. Merryfield, and W. G. Lee, 2012: The combined effect of tidally and eddy-driven diapycnal mixing on the large-scale ocean circulation. *J. Phys. Oceanogr.*, **42**, 526–538, doi:10.1175/JPO-D-11-0122.1.

Stommel, H., and A. B. Arons, 1960: On the abyssal circulation of the World Ocean—II. An idealized model of the circulation pattern and amplitude in oceanic basins. *Deep-Sea Res.*, **6**, 217–233, doi:10.1016/0146-6313(59)90075-9.

Talley, L. D., 2013: Closure of the global overturning circulation through the Indian, Pacific, and Southern Oceans: Schematics and transports. *Oceanography*, **26**, 80–97, doi:10.5670/oceanog.2013.07.

Viebahn, J., and C. Eden, 2010: Towards the impact of eddies on the response of the Southern Ocean to climate change. *Ocean Modell.*, **34**, 150–165, doi:10.1016/j.ocemod.2010.05.005.

Waterhouse, A. F., and Coauthors, 2014: Global patterns of diapycnal mixing from measurements of the turbulent dissipation rate. *J. Phys. Oceanogr.*, **44**, 1854–1872, doi:10.1175/JPO-D-13-0104.1.

Wolfe, C. L., and P. Cessi, 2010: What sets the strength of the middepth stratification and overturning circulation in eddying ocean models? *J. Phys. Oceanogr.*, **40**, 1520–1538, doi:10.1175/2010JPO4393.1.

——, and ——, 2011: The adiabatic pole-to-pole overturning circulation. *J. Phys. Oceanogr.*, **41**, 1795–1810, doi:10.1175/2011JPO4570.1.

Wunsch, C., and R. Ferrari, 2004: Vertical mixing, energy, and the general circulation of the oceans. *Annu. Rev. Fluid Mech.*, **36**, 281–314, doi:10.1146/annurev.fluid.36.050802.122121.